

Rh(0) nanoparticles as catalyst precursors for the solventless hydroformylation of olefins

Arnoldo J. Bruss^{a,b}, Marcos A. Gelesky^a, Giovanna Machado^a, Jairton Dupont^{a,*}

^a *Laboratory of Molecular Catalysis, Institute of Chemistry, UFRGS, Av. Bento Gonçalves 9500, Porto Alegre 91501-970, RS, Brazil*

^b *Universidad de Carabobo, Facultad de Ingeniería, Centro de Investigaciones Químicas, Valencia, Edo Carabobo, Venezuela*

Received 1 December 2005; received in revised form 16 January 2006; accepted 23 February 2006

Available online 3 April 2006

Abstract

The hydroformylation of 1-alkenes can be performed in solventless conditions using ligand-modified or unmodified Rh(0) nanoparticles prepared in imidazolium ionic liquids as catalyst precursors. There is a strong influence of the nanoparticle size on the hydroformylation reaction. Aldehydes are generated when 5.0 nm Rh(0) nanoparticles are used in the hydroformylation of 1-alkenes and *l/b* selectivities up to 25 can be achieved by addition of Xantphos (9,9-dimethyl-4,5-bis(diphenylphosphino)xanthene). Although small nanoparticles also generate catalytically active species the chemoselectivity decreases (around 11–17% of olefin isomerization) compared to those performed with the 5.0 nm nanoparticles. In contrast, the large sized nanoparticles (15 nm) produce only small amounts of aldehydes similar to that observed with a classical heterogeneous Rh/C catalyst precursor. TEM, XRD, IR and NMR experiments indicated that these Rh(0) nanoparticles are probably degraded under the reaction conditions into soluble mononuclear Rh-carbonyl catalytically active species.

© 2006 Elsevier B.V. All rights reserved.

Keywords: Nanoparticles; Rhodium; Hydroformylation; Metal-carbonyl; Surface

1. Introduction

The high surface area-to-volume ratio of solid-supported metal nanoparticles is mainly responsible for their catalytic properties and this can be exploited in many industrially important reactions [1]. Recently, it was found that soluble or non-supported nanoscale materials can in some cases give rise to novel and unique catalytic behaviour [2]. This has been possible, to a large extent, due to the significant recent advances in controlling synthetic pathways to metal nanoparticle. This has rendered possible a better fundamental understanding of the catalytic properties of metal nanoparticles by studying soluble or non-supported transition-metal nanoparticles as “model” materials [3–7]. In this respect, it is expected that transition-metal nanoparticles of 1–10 nm in size will exhibit physical–chemical properties intermediate between those of the smallest element from which they can be composed and those of the bulk material [8]. Indeed, in many cases this new generation of nanopar-

ticles gives rise to unique catalytic activities/selectivities and their metal-surface properties can be modulated by the addition of ligands, for example Ref. [9]. However, in other cases these nanomaterials behave like classical heterogeneous catalysts [10–12] and in some other cases these soluble materials are degraded, under the reaction conditions, generating monometallic homogenous catalytically active species [13].

The hydroformylation of olefins is catalyzed by a plethora of monometallic complexes modified or not by several different types of ligands [14–16]. Molecular clusters have also been investigated but under the hydroformylation conditions these multinuclear compounds degraded into at least bimetallic species, which promote the reaction [17–23]. For example, multinuclear compounds such as $[\text{Rh}_4(\text{CO})_{12}]$ and $[\text{Rh}_6(\text{CO})_{16}]$ are transformed into $[\text{RhH}(\text{CO})_3]$, which is responsible for the catalytic activity [24,25]. Therefore, the hydroformylation of olefins can constitute a chemical reaction probe for investigating the properties of transition-metal nanoparticles, i.e., if they possess typical molecular metal cluster or surface-like catalytic properties. We wish to disclose herein our results concerning the catalytic properties of Rh(0) nanoparticles in the solventless hydroformylation of olefins in the presence and absence of

* Corresponding author. Tel.: +55 51 33166321; fax: +55 51 33167304.

E-mail address: dupont@iq.ufrgs.br (J. Dupont).

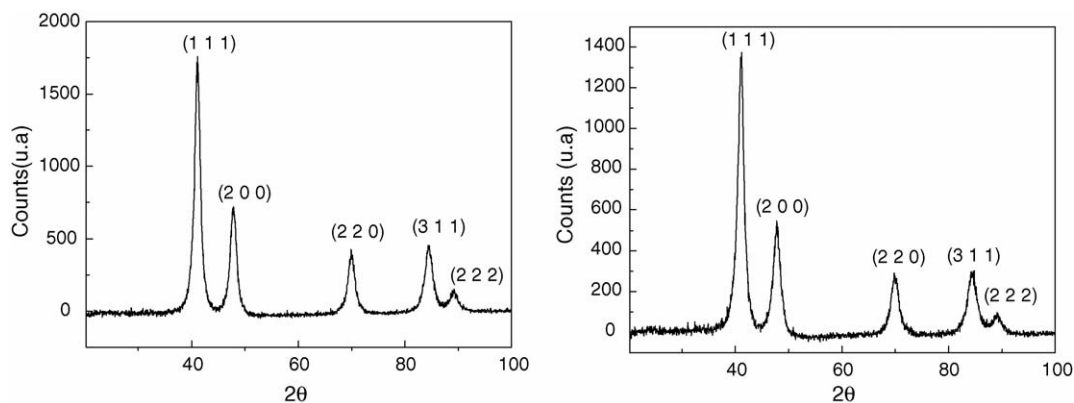


Fig. 1. X-ray diffraction pattern of the isolated Rh(0) nanoparticles dispersed in BMI-BF₄ before (left) and after (right) the hydroformylation reaction.

Xantphos (9,9-dimethyl-4,5-bis(diphenylphosphino)xanthene) [26].

2. Results and discussion

The Rh(0) nanoparticles were prepared by simple hydrogen reduction of RhCl₃·nH₂O dissolved in 1-*n*-butyl-3-methylimidazolium tetrafluoroborate (BMI·BF₄) ionic liquid

[27] using a similar experimental protocol recently developed for the preparation of various stable transition-metal nanoparticles [28]. The Rh(0) nanoparticles were isolated by centrifugation, washed with methanol, dried under reduced pressure and analyzed by X-ray powder (XRD) diffraction and transmission electron microscopy (TEM).

The XRD pattern (Fig. 1) confirmed the crystalline Rh(0) and it was adjusted by indexation of five Bragg reflections corre-

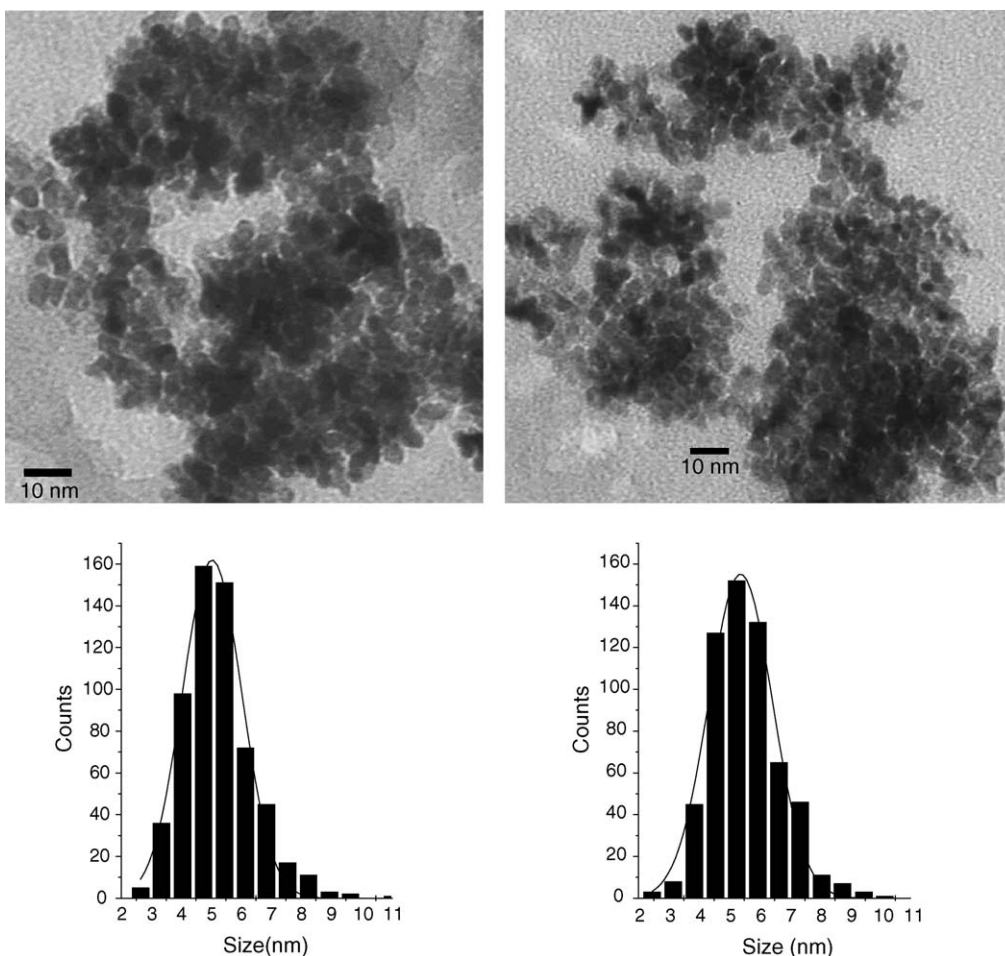


Fig. 2. Parts of the transmission electron micrograph and histograms illustrating the particle size distribution of the Rh(0) nanoparticles dispersed in BMI-BF₄ before (left) and after the hydroformylation reaction (right).

sponding to the Rh(0) (1 1 1), (2 0 0), (2 2 0), (3 1 1) and (2 2 2) as face-centered cubic (fcc) with lattice parameter $a = 3.8028$. A mean diameter of 4.6 nm could be estimated from the XRD diffraction pattern by means of the Debye-Scherrer equation (using the parameters obtained with Rietveld's refinements) which corresponds well with the average diameter of 5.0 ± 1.0 nm determined from TEM images (see below).

The size and morphology of the Rh(0) nanoparticles in the ionic liquid were also investigated in situ by TEM analysis. The nanoparticle-size distribution was estimated from the measurement of about 600 particle diameters, assuming a spherical shape, found in an arbitrary chosen area in enlarged microphotographs (Fig. 2). These particles display a monomodal size distribution with an average diameter of 5.0 ± 1.0 nm.

The isolated Rh(0) nanoparticles were mixed with 1-hexene, 1-octene or 1-decene in an autoclave and a CO/H₂ mixture (50 bar, 1:1) was admitted to the system at 100 °C and 660 rpm stirring rate. Note that these reactions are performed in a typical "solventless" condition where the substrates and products are per-definition the solvent(s) of the catalytic process. The fall in the syngas pressure in the autoclave was monitored with a pressure transducer interfaced with a PC. The olefin consumption and the formation of the products were also followed by GC and GC-MS. At the end of the reaction the nanoparticles were easily separated as a black powder by a simple decantation procedure.

The conversion of the olefins during the hydroformylation reaction is presented in Fig. 3. The results obtained under different conditions are summarized in Table 1. In all experiments, induction periods of 1–4 h (not shown in Fig. 3) were observed indicating the transformation of the nanoparticles into catalytically active species.

Aldehydes were the major products observed in all reactions without any trace of hydrogenation products (Scheme 1), except in the reactions performed with large Rh nanoparticles or Rh/C (entries 5–7, Table 2). This is quite surprising since Rh(0)

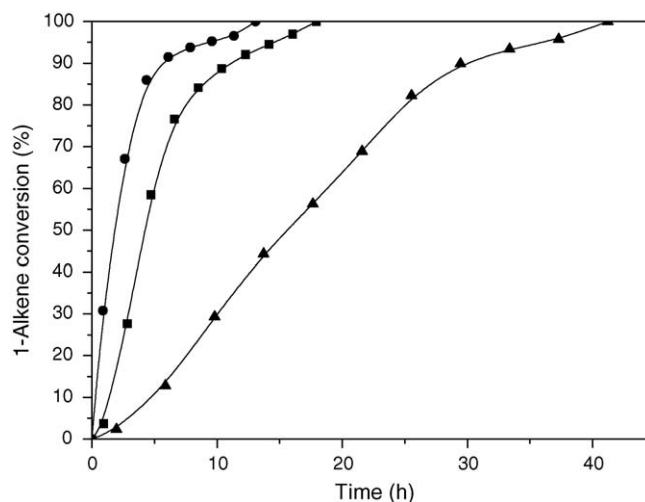


Fig. 3. Hydroformylation of 1-hexene (▲), 1-octene (■) and 1-decene (●) (10 mmol) by Rh(0) nanoparticles (5 mg) at 100 °C and 50 atm of CO/H₂ (1/1).

nanoparticles are highly active catalysts for the hydrogenation of olefins [29].

The mean diameter of 4.8 nm estimated from the XRD diffraction pattern by means of the Debye-Scherrer equation of the isolated metal particles from the ionic liquid after the hydroformylation indicated no modification on their size. However, the recovered nanoparticles analyzed by TEM (Fig. 2) showed a significant narrowing of overall particle size with a slight increase of particle size, in particular those with 5–6 nm (see histograms in Fig. 2). Indeed, a mean diameter of 5.4 ± 1.0 nm was estimated from the measurement of about 600 particle diameters, assuming a spherical shape, found in an arbitrary chosen area in enlarged microphotographs of the Rh(0) in the ionic liquid after the hydroformylation of 1-hexene. This process is typical of an Ostwald ripening-type mechanism, i.e., the growth

Table 1
Hydroformylation of olefins by Rh(0) nanoparticles^a

Entry	Catalyst	Olefin	t (h) ^b	cv. (%) ^c	l/b ^d	Is. ^e (%)	It. ^f (h)
1	Rh(0)	1-Decene	18	100	1.5	<1	2.5
2	Rh(0)	1-Octene	13	100	1.7	<1	<1
3	Rh(0)	1-Hexene	41	100	1.8	<1	2.0
4	Rh from 3	1-Hexene	6	100	1.8	<1	<1
5	Rh from 4	1-Hexene	19	100	1.5	<1	<1
6	Rh from 5	1-Hexene	19	100	1.3	<1	1.0
7	Rh from 6	1-Hexene	21	100	1.5	<1	<1
8	Rh from 7	1-Hexene	19	98	1.4	<1	<1
9	Org. phase from 3	1-Hexene	16	100	1.8	<1	<1
10	Rh(0)/Xantphos ^g	1-Hexene	30	100	25	<1	4.0
11	Org. phase from 10	1-Hexene	18	97	2.0	<1	<1

^a Reaction conditions: Rh(0) (5 mg); olefin (10 mmol); CO/H₂ (1/1, 50 bar); and $T = 100$ °C.

^b Time for the CO/H₂ consumption without the induction time.

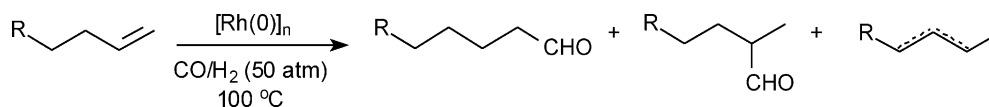
^c Olefin conversion.

^d Ratio linear/branched aldehydes.

^e Percentage of internal olefins.

^f Induction time required for the beginning of CO/H₂ consumption.

^g Xantphos (10 mg, 0.017 mmol).



Scheme 1.

Table 2
Hydroformylation of olefins by Rh(0) nanoparticles with different sizes and Rh/C^a

Entry	Catalyst	Olefin	<i>t</i> (h) ^b	cv. (%) ^c	<i>l/b</i> ^d	Is. ^e (%)	It. ^f (h)
1	Rh(0) (5.0 nm)	1-Decene	18	100	1.5	<1	2.5
2	Rh(0) (5.0 nm)	1-Hexene	41	100	1.8	<1	2.0
3	Rh(0) (2.7 nm)	1-Hexene	23	93	1.9	17	3.0
4	Rh(0) (2.7 nm)	1-Decene	40	92	0.5	11	2.0
5	Rh(0) (15 nm)	1-Decene	22	4	1.1	2	4.0
6	Rh(0) (15 nm)	1-Decene	46	72	2.0	54	3.5
7	Rh/C (5%)	1-Hexene	20	21	1.5	16	2.0

^a Reaction conditions: Rh(0) (5 mg); olefin (10 mmol); CO/H₂ (1/1, 50 bar); and *T* = 100 °C.

^b Time for the CO/H₂ consumption without the induction time.

^c Olefin conversion.

^d Ratio linear/branched aldehydes.

^e Percentage of internal olefins.

^f Induction time required for the beginning of CO/H₂ consumption.

of larger nanoparticles from those of smaller size which have a higher solubility than the larger ones. Moreover, this process may explain the presence of monometallic rhodium species in solution during the hydroformylation reaction (see below).

The recovered nanoparticles could be re-used five times without significant changes in their catalytic activities (see entries 4–8, Table 1). The *l/b* ratio (1.1–1.8) obtained with the nanoparticles is the same as the one usually obtained with unmodified rhodium complexes under homogeneous or biphasic conditions [15]. Note that the 1-hexene hydroformylation is slower in the first run (Table 1, entry 3) than the recharges using the recovery Rh(0) nanoparticles (Table 1, entries 4–6). This is probably due to the presence of more exposed surface atoms after the first hydroformylation run. However, the mixture of solid Xantphos and Rh(0) nanoparticles also gives rise to only aldehyde products but a *l/b* (linear/branched) ratio of 25 (entry 10, Table 1) typical of Rh-Xantphos molecular catalysts.[26] This suggests the possible formation of modified Xantphos nanoparticle species and/or the degradation of the nanoparticles with the formation of molecular Rh-Xantphos complexes that are in fact the catalytically active species.

In order to verify these hypotheses the recovered organic phase of the unmodified Rh nanoparticles was used as a catalyst precursor for the hydroformylation of 1-hexene (entry 9, Table 1) and hydroformylation occurred with a 1.8 *l/b* selectivity. Even though the catalytic activity of this organic phase was modest compared to that observed with the recovered nanoparticles (entry 4, Table 1) this is an indication of the presence of soluble Rh species (Fig. 4).

The appearance, in the IR spectra, in an organic solution, of a weak stretching band at 1814 cm⁻¹ (besides the CO stretching band of the aldehydes at 1780 and 1790 cm⁻¹) is an indication of the presence of a carbonyl ligand attached to a Rh cluster nucleus. Rh ionic species was not observed by ESI-MS in both positive and negative modes of the organic phase. We have also

checked the organic phase of the reaction performed in the presence of Xantphos (entry 11, Table 1) by ³¹P-¹H NMR. The ³¹P-¹H NMR spectrum shows only two broad singlets at 28.7 and 30.2 ppm, which can be attributed to the Xantphos associated with Rh-carbonyl compounds. Interestingly, the addition of Xantphos to the organic phase recovered from the hydroformylation of 1-hexene promoted by Xantphos-Rh nanoparticles suppresses the catalytic activity of this solution. Moreover, the ³¹P-¹H NMR spectrum of a mixture of Rh(0) nanoparticles, Xantphos and aldehyde shows two relatively broad peaks centered at 32 ppm and no peak corresponding to free-Xantphos was observed, suggesting that all the Xantphos ligand interacts with the Rh centers. The IR spectra of the Rh(0) nanoparticles (CaF₂ pellets) under 1 bar of CO during 20 h shows bands at 2088 and 2019 cm⁻¹ (Fig. 5) characteristic of Rh(CO)₂ species

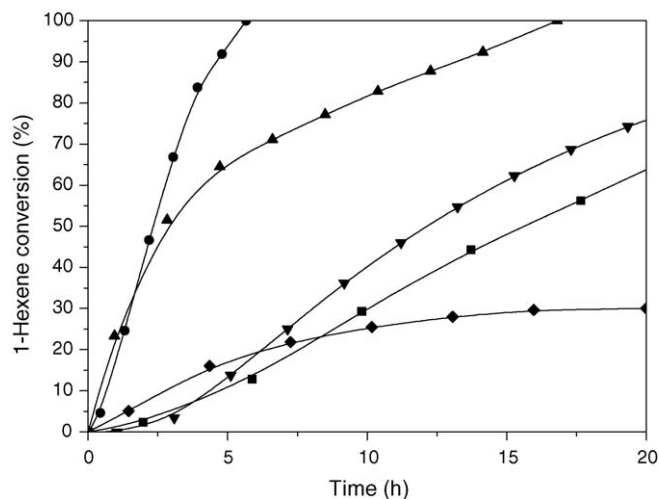


Fig. 4. Hydroformylation of 1-hexene by Rh(0) nanoparticles and Rh/C. (■) Rh(0) (5.0 nm) first run; (●) Rh(0) recovered; (▲) organic phase recovered; (▼) Rh(0)/Xantphos; (◆) Rh/C.

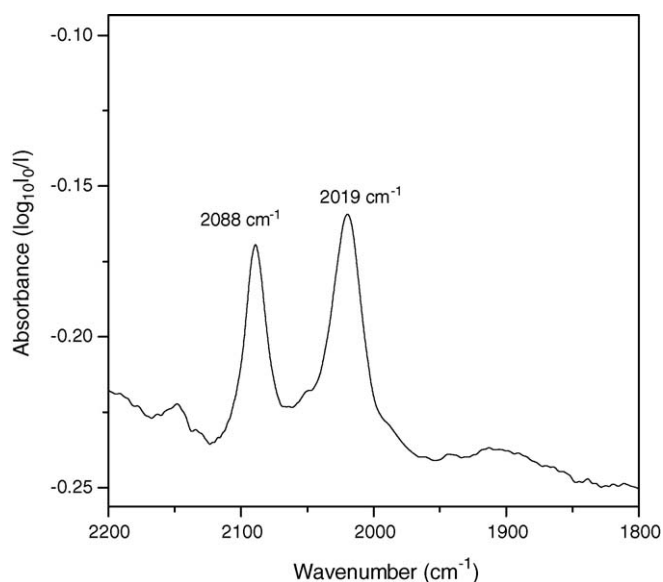


Fig. 5. Part of the IR spectra of the Rh(0) nanoparticles (CaF₂ pellets) under 1 bar of CO (20 h).

present in Rh surfaces covered by CO [30]. The same IR spectrum was obtained for the Rh nanoparticles under 1 bar of CO/H₂ (1/1) during 24 h.

We have also tested smaller (2.7 nm) [11] and larger (15 nm) [31] Rh(0) nanoparticles prepared by hydrogen reduction of RhCl₃·nH₂O and [RhCl(cod)]₂, respectively, dissolved in 1-*n*-butyl-3-methylimidazolium hexafluorophosphate ionic liquid (see Table 2).

There is a strong influence of the nanoparticle size on the hydroformylation reaction: although small nanoparticles also generate catalytically active species the chemoselectivity decreases (around 11–17% of olefin isomerization) compared to those performed with the 5.0 nm nanoparticles. In contrast, the large sized nanoparticles produce only small amounts of aldehydes similar to that observed with a classical heterogeneous Rh/C catalyst precursor (compare entries 5–6 and 7, Table 2). It is obvious that the lower catalytic activity observed with the large sized nanoparticles is related with the presence of less Rh atoms on the surface than those with 5.0 nm. It is also important to note that the isolated nanoparticles prepared either in 1-*n*-butyl-3-methylimidazolium tetrafluoroborate or hexafluorophosphate contains residual ionic liquids on their surfaces as observed by XPS analysis [31,32]. Therefore, the higher catalytic activity obtained with the 5.0 nm nanoparticles (prepared in 1-*n*-butyl-3-methylimidazolium tetrafluoroborate) compared to those obtained with the 2.7 and 15 nm (both prepared in 1-*n*-butyl-3-methylimidazolium hexafluorophosphate) can be also due to the presence of more exposed Rh atoms on their surface since BF₄ anion is much less coordinating than PF₆ anion [33].

3. Conclusions

We demonstrated that unmodified or ligand-modified 5.0 nm Rh(0) nanoparticles are catalyst precursors for the hydroformylation of 1-alkenes. Although at this stage of our studies we

cannot exclude that the hydroformylation reaction occurs at the nanoparticle surface, most of the data including the induction periods observed in all reactions starting from the nanoparticles are indicative of nanoparticle degradation under the reaction conditions into soluble mononuclear Rh-carbonyl catalytically active species as observed earlier in the reactions performed with Rh-carbonyl molecular clusters [17]. However, whatever the path involved in the formation of the catalytically active species it is clear that it depends on the size of the starting Rh nanoparticles.

4. Experimental

4.1. General

All reactions were performed under an argon atmosphere using Schlenk techniques. The substrates (Acros or Aldrich) were obtained from commercial sources and used as received. The ionic liquids were prepared according to known procedures [27], dried over molecular sieves (4 Å) and their purity was checked by an AgNO₃ test, ¹H and ¹³C NMR, and Cyclic Voltametry. The water [34] (<0.1 wt%) and chloride [35] (<1.4 mg/L) contents in the ionic liquids used were determined by known methods. NMR analyses were performed on a Varian Inova 300 spectrometer. Infrared spectra were obtained on a Bomem B-102 spectrometer.

4.2. XRD analysis of the isolated nanoparticles

For the XRD analyses the nanoparticles were isolated as a fine powder and placed in the sample holder. The wide angle X-ray diffraction (WAXD) experiments were carried out on a SIEMENS D500 diffractometer equipped with curved graphite crystal using Cu Kα radiation (λ = 1.5406 Å). The diffraction data were collected at room temperature in a Bragg-Brentano θ–2θ geometry. The equipment was operated at 40 kV and 20 mA with scan range between 10° and 100°. The diffractograms were obtained with a constant step 0.05. The Rietveld's refinement (Fig. 6) was obtained using the FULLPROF code.

4.3. TEM analysis

The nanoparticle size and morphology of the particles isolated before and after hydroformylation reaction were investigated in situ by TEM analysis carried out directly on the ionic liquid nanoparticle-containing phase. The morphologies of the obtained particles were carried out on a JEOL JEM-2010 equipped with an energy dispersive X-ray spectroscopy (EDS) system and JEOL JEM-1200 EXII electron microscope operating at an accelerating voltage of 200 and 120 kV, respectively. The samples for TEM were prepared by deposition on a carbon-coated copper grid of the rhodium nanoparticles dispersed in the ionic liquid at room temperature. The histograms of the nanoparticles size distribution were obtained from measurement of about 300 particles (600 counts), and were reproduced in different regions of the Cu grid, assuming spherical shape, found in an arbitrary chosen area of enlarged micrographs. The HRTEM

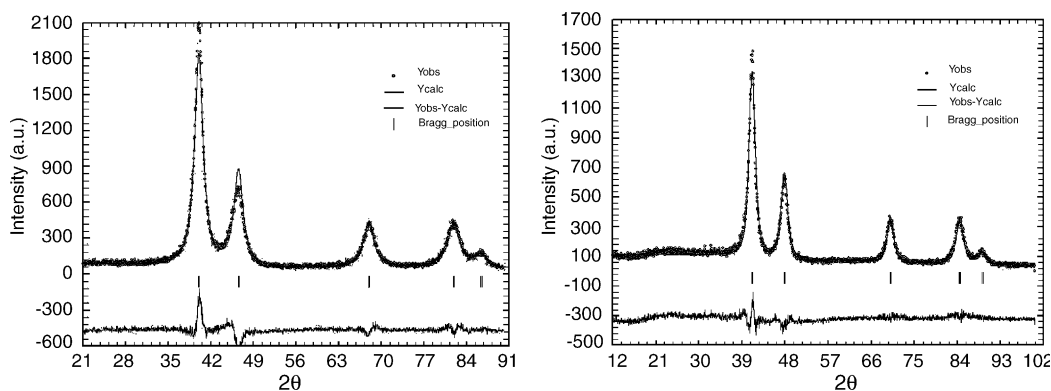


Fig. 6. Rietveld's refinement of X-ray diffraction patterns of the Rh(0) nanoparticles before (left) and after (right) the hydroformylation reaction.

images (Fig. 7) were analyzed by in Gatan Software from which it was obtained the Fourier transformed.

4.4. Nanoparticle formation and isolation

In a typical experiment, a Fischer Porter bottle containing a red solution of $\text{RhCl}_3 \cdot x\text{H}_2\text{O}$ (26 mg, 0.1 mmol) in methanol (5 mL) was added to $\text{BMI} \cdot \text{BF}_4$ (1 mL) and stirred at room temperature for 15 min. The volatiles were then removed under reduced pressure (0.1 bar) at 75°C for 1 h. The system was kept at 75°C and hydrogen (4 bar) was admitted to the system. After stirring for 1 h a black solution was obtained and 15 mL of methanol were added and the nanoparticles were isolated by centrifugation (3000 rpm) for 5 min and washed with methanol (3×15 mL) and dried under reduced pressure. The Rh samples thus obtained were prepared for TEM and X-ray analysis, and for catalytic experiments.

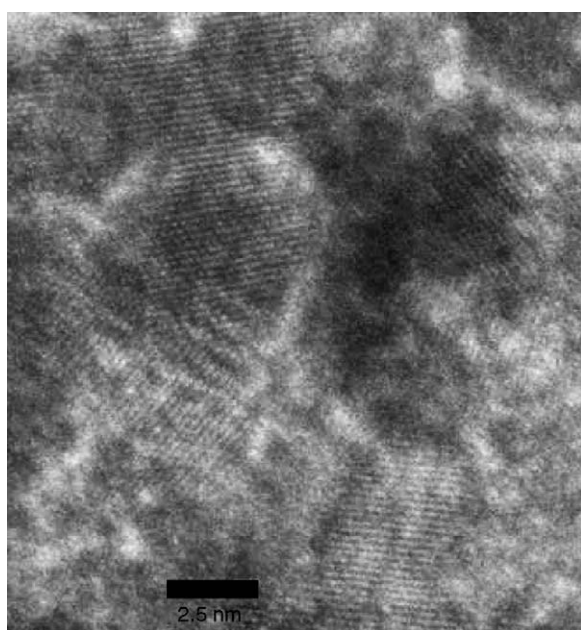


Fig. 7. High resolution transmission electron micrograph (HRTEM) of the Rh(0) nanoparticles dispersed in $\text{BMI} \cdot \text{BF}_4$ before the hydroformylation reaction.

4.5. Catalytic experiments

Catalytic experiments were performed in a 50 mL capacity stainless-steel reaction vessel (Parr) using a mechanic stirrer (660 rpm). The fall in the CO/H_2 pressure in the reaction vessel was monitored with a pressure transducer interfaced through a Novus converter to a PC and the data workup via Microcal Origin 5.0. The Rh(0) nanoparticles (5 mg) and the desired olefin (10 mmol) were transferred under argon to the reaction vessel. Thereafter, the reaction vessel was pressurized with 50 bar of CO/H_2 (1/1) and the reaction was initiated by placing the reaction vessel into a temperature-controlled oil bath preheated at 100°C . Catalytic reactions were terminated by removing the vessel from the oil bath and depressurized after cooling in an ice bath. In all cases the organic layer was readily separated from the solid nanoparticles. The organic phase was analyzed by GC using a Varian gas chromatograph with a FID and 30 m long capillary column with a dimethylpolysiloxane stationary phase and using di-*n*-butyl ether as standard. The organic compounds were characterized by GC–MS and by comparison of their GC retention times with those of authentic samples.

Acknowledgements

Thanks are due to the following Brazilian agencies: CNPq, CAPES and CT-PETRO for partial financial support.

References

- [1] R.A. Van Santen, P.W.N.M. Van Leeuwen, J.A. Moulijn, B.A. Averill (Eds.), *Catalysis: An Integrated Approach*, second, revised and enlarged edition [in: *Stud. Surf. Sci. Catal.* (1999) 123], Elsevier, Amsterdam, 1999.
- [2] M. Valden, X. Lai, D.W. Goodman, *Science* 281 (1998) 1647.
- [3] L.N. Lewis, *Chem. Rev.* 93 (1993) 2693.
- [4] M. Kralik, A. Biffis, *J. Mol. Catal. A: Chem.* 177 (2001) 113.
- [5] J.D. Aiken, R.G. Finke, *J. Mol. Catal. A: Chem.* 145 (1999) 1.
- [6] A. Roucoux, J. Schulz, H. Patin, *Chem. Rev.* 102 (2002) 3757.
- [7] H. Bonnemann, R.M. Richards, *Eur. J. Inorg. Chem.* (2001) 2455.
- [8] A.T. Bell, *Science* 299 (2003) 1688.
- [9] S. Jansat, M. Gomez, K. Philippot, G. Muller, E. Guiu, C. Claver, S. Castillon, B. Chaudret, *J. Am. Chem. Soc.* 126 (2004) 1592.

- [10] G.S. Fonseca, E.T. Silveira, M.A. Gelesky, J. Dupont, *Adv. Synth. Catal.* 347 (2005) 847.
- [11] G.S. Fonseca, A.P. Umpierre, P.F.P. Fichtner, S.R. Teixeira, J. Dupont, *Chem. Eur. J.* 9 (2003) 3263.
- [12] E.T. Silveira, A.P. Umpierre, L.M. Rossi, G. Machado, J. Morais, G.V. Soares, I.L.R. Baumvol, S.R. Teixeira, P.F.P. Fichtner, J. Dupont, *Chem. Eur. J.* 10 (2004) 3734.
- [13] C.C. Cassol, A.P. Umpierre, G. Machado, S.I. Wolke, J. Dupont, *J. Am. Chem. Soc.* 127 (2005) 3298.
- [14] P.C.J. Kamer, A. van Rooy, G.C. Schoemaker, P.W.N.M. Van Leeuwen, *Coord. Chem. Rev.* 248 (2004) 2409.
- [15] P.W.N.M. Van Leeuwen, C. Claver, *Compr. Coord. Chem. II* 9 (2004) 141.
- [16] H.-W. Bohnen, B. Cornils, *Adv. Catal.* 47 (2002) 1.
- [17] D.T. Brown, T. Eguchi, B.T. Heaton, J.A. Iggo, R. Whyman, *J. Chem. Soc. Dalton Trans.* (1991) 677.
- [18] I.T. Horvath, M. Garland, G. Bor, P. Pino, *J. Organomet. Chem.* 358 (1988) C17.
- [19] A. Ceriotti, L. Garlaschelli, G. Longoni, M.C. Malatesta, D. Strumolo, A. Fumagalli, S. Martinengo, *J. Mol. Catal.* 24 (1984) 309.
- [20] A.D. Harley, G.J. Guskey, G.L. Geoffroy, *Organometallics* 2 (1983) 53.
- [21] C.Z. Li, E. Widjaja, M. Garland, *Organometallics* 23 (2004) 4131.
- [22] C.Z. Li, E. Widjaja, M. Garland, *J. Am. Chem. Soc.* 125 (2003) 5540.
- [23] G.W. Liu, M. Garland, *J. Organomet. Chem.* 613 (2000) 124.
- [24] M. Garland, *Organometallics* 12 (1993) 535.
- [25] C. Fyhr, M. Garland, *Organometallics* 12 (1993) 1753.
- [26] M. Kranenburg, Y.E.M. Vanderburgt, P.C.J. Kamer, P. Vanleeuwen, K. Goubitz, J. Fraanje, *Organometallics* 14 (1995) 3081.
- [27] P.A.Z. Suarez, J.E.L. Dullius, S. Einloft, R.F. DeSouza, J. Dupont, *Polyhedron* 15 (1996) 1217.
- [28] J. Dupont, G.S. Fonseca, A.P. Umpierre, P.F.P. Fichtner, S.R. Teixeira, *J. Am. Chem. Soc.* 124 (2002) 4228.
- [29] G.S. Fonseca, A.P. Umpierre, P.F.P. Fichtner, S.R. Teixeira, J. Dupont, *Chem. Eur. J.* 9 (2003) 3263.
- [30] J.T. Yates, T.M. Duncan, S.D. Worley, R.W. Vaughan, *J. Chem. Phys.* 70 (1979) 1219.
- [31] M.A. Gelesky, A.P. Umpierre, G. Machado, R.R.B. Correia, W.C. Magno, J. Morais, G. Ebeling, J. Dupont, *J. Am. Chem. Soc.* 127 (2005) 4588.
- [32] A.P. Umpierre, G. Machado, G.H. Fecher, J. Morais, J. Dupont, *Adv. Synth. Catal.* 347 (2005) 1404.
- [33] J. Dupont, *J. Braz. Chem. Soc.* 15 (2004) 341.
- [34] B.K. Sweeny, D.G. Peters, *Electrochem. Commun.* 3 (2001) 712.
- [35] V. Gallo, P. Mastroilli, C.F. Nobile, G. Romanazzi, G.P. Suranna, *J. Chem. Soc. Dalton Trans.* (2002) 4339.